2009

Magnetic phase transitions in Pr1-xLuxMn2Ge2 compounds

S X. Dou
University of Wollongong, shi@uow.edu.au

Jianli Wang
University of Wollongong, jianli@uow.edu.au

Maxim Avdeev
ANSTO

A J Studer
ANSTO

Rong Zeng
University of Wollongong, rzeng@uow.edu.au

See next page for additional authors

Magnetic Phase Transitions in $Pr_{1-x}Lu_xMn_2Ge_2$ Compounds

J.L. Wang[a,b,c], S.J. Campbell[a], A.J. Studer[b], M. Avdeev[b], R. Zeng[c] and S.X. Dou[c]

[a]School of Physical, Environmental and Mathematical Sciences,

The University of New South Wales, The Australian Defence Force Academy,

Canberra ACT 2600, Australia

[b]Bragg Institute, ANSTO, Lucas Heights, NSW 2234 Australia

[c]Institute for Superconductivity and Electronic Materials, University of Wollongong,

Wollongong, NSW 2522 Australia

The effects of replacing Pr by Lu on the magnetic behaviour and structures in $Pr_{1-x}Lu_xMn_2Ge_2$ (x=0.2, x=0.4) have been investigated using X-ray diffraction, Mössbauer spectroscopy, magnetisation and neutron diffraction measurements. The substitution of Lu for Pr leads to a decrease in the lattice constants *a*, *c* and the unit cell volume V at room temperature with this contraction of the unit cell resulting in modifications of the $Pr_{1-x}Lu_xMn_2Ge_2$ magnetic structures. Four and five magnetic phase transitions - linked primarily with temperature driven changes in the intralayer Mn-Mn separation distances - have been detected within the temperature range 4.5 – 550 K for $Pr_{0.8}Lu_{0.2}Mn_2Ge_2$ and $Pr_{0.6}Lu_{0.4}Mn_2Ge_2$, respectively with re-entrant ferromagnetism being detected around T_C^{Pr} ~ 31 K for $Pr_{0.6}Lu_{0.4}Mn_2Ge_2$. It was found that T_C^{inter} and T_C^{Pr} increase with increasing applied field while T_N^{inter} decreases for $Pr_{0.6}Lu_{0.4}Mn_2Ge_2$ indicating that the canted antiferromagnetic AFmc region contracts with increasing field. The Debye temperatures for $Pr_{1-x}Lu_xMn_2Ge_2$ with x=0.2 and 0.4 were evaluated as θ_D = 320 ±40 K and θ_D = 400 ±20 K respectively from the temperature dependence of the average isomer shift. The magnetic structures of both compounds have been determined by neutron diffraction measurements over the temperature range 3 - 300 K with formation of the Fmi magnetic state below $T_{c/c}$ = 192 K for $Pr_{0.8}Lu_{0.2}Mn_2Ge_2$ and the occurrence of re-entrant ferromagnetism below T_C^{Pr} = 31 K for $Pr_{0.6}Lu_{0.4}Mn_2Ge_2$ being confirmed.

Key words: Magnetic phase transition, Magnetic susceptibility, Mössbauer spectroscopy, Intrinsic properties of magnetically ordered materials

PACS: 75.30.Kz, 75.30.Cr, 76.80.+y, 75.30.-m

1. Introduction

The magnetic properties of the ternary rare-earth RMn_2Ge_2 compounds with the tetragonal $ThCr_2Si_2$-type structure (I4/mmm) have continued to attracted interest in recent years; this is linked in part to their natural multilayer structure which can exhibit either coupled magnetic and crystallographic transitions or valence-related transitions [e.g. 1-5] and also plays a role in materials which exhibit a giant magnetocaloric effect (GMCE). It is well known that the main driving mechanism for the magnetism of these 1-2-2 type compounds is the strong dependence of Mn-Mn intraplanar and interplanar exchange interactions on $d^a_{Mn\text{-}Mn}$, the Mn-Mn separation distance in the *ab*-plane [6, 7]. Recently, it was reported that several compounds with a distinct layered structure exhibit a giant magnetocaloric effect (GMCE) such as $Gd_5Si_2Ge_2$ [8], $RTi_{1-x}Mo_xGe$ (R = Tb, Er; x = 0, 0.15) [9] and $R_{1-x}M_xMnO_3$(R=La, Nd, Pr and M= Ca, Sr, Ba, etc.) [10], where interlayer distances play a vital role in determining their magnetic phase transition order/type and in governing the MCE performance. The strong dependence of the interlayer exchange interaction in RMn_2Ge_2 on the distance between magnetic atoms in layered compounds [2, 11, 12] is expected to offer scope for selection of the magnetic state - and therefore the MCE - by controlling the interlayer and intralayer distances between magnetic atoms using chemical (*i.e.* brought about by compositional changes) or external pressure [13]. Indeed, recently it has been confirmed that the Sm-Mn coupling plays a crucial role in determining the magnitude of magnetocaloric properties in $SmMn_2Ge_2$ both at ambient and under applied pressures [14].

Here, we investigate the effects on the magnetic structure of substituting Lu for Pr in $Pr_{1-x}Lu_xMn_2Ge_2$ (x = 0.2, 0.4) for the first time using magnetic, Mössbauer spectroscopy and neutron diffraction measurements. In addition to exploring the effects of the non magnetic Lu atoms on the rare earth Pr sublattice, it is expected that substitution of Pr (atomic radius 1.82 Å) with the smaller Lu (atomic radius 1.75 Å) would modify the magnetic structure of $Pr_{1-x}Lu_xMn_2Ge_2$. This follows as $d^a_{Mn\text{-}Mn}$ ~ 2.915 Å in $PrMn_2Ge_2$ [15] while $d^a_{Mn\text{-}Mn}$ ~ 2.785 Å in $LuMn_2Ge_2$ [7]. These values of

$d^a_{Mn\text{-}Mn}$ are respectively greater than d_{crit1}~2.87 Å and less than d_{crit2} ~2.84 Å, the first and second critical intralayer Mn-Mn distances which govern the magnetic behaviour in RMn_2Ge_2 compounds [6, 7]. According to Welter *et al.* [15], the $d^a_{Mn\text{-}Mn}$ not only affects the intralayer Mn-Mn coupling but also the interlayer exchange interaction and three general categories can be delineated [6, 13]:

(i) The interlayer exchange coupling being ferromagnetic and the intralayer coupling antiferromagnetic for $d^a_{Mn\text{-}Mn} > d_{crit1}$=2.87 Å leading to the canted Fmc-type ferromagnetic structure.

(ii) Both the interlayer and the intralayer coupling being antiferromagnetic (AFmc-type magnetic structure) for d_{crit2}=2.84 Å < $d^a_{Mn\text{-}Mn}$ < d_{crit1}=2.87 Å.

(iii) No intralayer in-plane spin component and the interlayer coupling being antiferromagnetic, leading to the AFil-type magnetic structure $d^a_{Mn–Mn}$ in the range $d^a_{Mn\text{-}Mn}$ < d_{crit2}=2.84 Å [6, 13].

In order to aid discussion of the magnetic behaviours observed in this study, several of the relevant Mn sublattice magnetic structures are depicted in Fig. 1 with the notation used to describe the magnetic structure types and critical transition temperatures defined in [7]. Magnetic transition from paramagnetic (P) to intralayer anti-ferromagnetic ordering within the (001) Mn layers (AFl) at T_N^{intra} = 415 K has been reported in $PrMn_2Ge_2$ (lattice parameter *a*=4.123 Å at room temperature) [15] and below T_C^{inter}=334 K a canted spin structure (Fmc) with the c-axis interlayer spin components aligning parallel and anti-ferromagnetic ordering within the (001) Mn layers is formed. With further decrease in temperature to below $T_{c/c}$ = 280 K the structure transforms from Fmc to a conical configuration (Fmi) and below about 100 K, the Pr sublattice in $PrMn_2Ge_2$ orders magnetically along the c-axis with the Pr moments coupled parallel to the Mn moments (Fmi + F(Pr)). With $LuMn_2Ge_2$ (lattice parameter *a*=3.939 Å at room temperature) found to exhibit the antiferromagnetic interlayer coupling structure AFil below T_N= 508 K [7], it is clear that a variety of interesting magnetic phenomena can be expected on substituting Lu for Pr in $Pr_{1-x}Lu_xMn_2Ge_2$.

Here we investigate $Pr_{1-x}Lu_xMn_2Ge_2$ compounds with x=0.2 and 0.4, using magnetic, Mössbauer and neutron diffraction measurements.

2. Experimental

$Pr_{1-x}Lu_xMn_2Ge_2$ (^{57}Fe) compounds with x = 0.2 and 0.4 were prepared by conventional argon arc melting. The starting materials contained ~3% excess Mn to compensate for the Mn loss due to evaporation during melting and the ingot was melted five times for improved homogeneity. The samples were doped with ~ 0.5 wt% ^{57}Fe for the Mössbauer studies and the samples were characterized by x-ray diffraction (CuK_α radiation; λ = 1.5418 Å). The temperature dependence of the magnetisation, M (T), was measured in a magnetic field of B_{appl} = 0.005 T in a superconducting quantum interference device (SQUID) from 5 K to 350 K. The differential scanning calorimetry (DSC) measurements have been measured to check for possible phase transitions in the higher temperature range from 300 K to 550 K. The transition temperatures T_C^{Pr} and T_N^{inter} for compounds were defined as the temperatures at which dM/dT exhibits an extreme value [16] while the magnetic transition temperatures T_C^{inter} were derived from the thermal magnetic curves by extrapolating M^2–T plots to $M^2 = 0$ [17]. The ^{57}Fe Mössbauer spectra were obtained between 4.2 K and 298 K using a standard constant-acceleration spectrometer and a ^{57}Co**Rh** source. The spectrometer was calibrated at room temperature with an α-iron foil. Neutron diffraction experiments were carried out on the powder samples using the MRPD diffractometer (λ = 1.6660 Å) of Reactor HIFAR (shut down in January 2007 after 50 years of safe operation), Lucas Heights, and the high intensity diffractometer Wombat (λ = 2.410 Å) of Australia's Replacement Research Reactor OPAL, Lucas Heights at temperatures over the range 3-300 K.

3. Results and Discussion

X-ray diffraction patterns indicate that the compounds have a single phase with the tetragonal $ThCr_2Si_2$-type structure (space group I4/mmm, space group number 139). The patterns have been analysized using the FULLPROF software and the lattice parameters have been obtained (listed in Table 1). The replacement of Pr with Lu leads to the expected decrease in lattice parameters due to smaller atomic size of Lu than Pr. The bond lengths between different sites have also been calculated with the BLOKJE program [18] using the structural and positional parameters and the 12-coordinate metallic radii of 1.82 Å, 1.75 Å, 1.35 Å and 1.37 Å for Pr, Lu, Mn and Ge, respectively.

It can be seen from Table 1 that, with increasing Lu content, the intralayer Mn-Mn spacing $d^a_{Mn\text{-}Mn}$ at room temperature for $Pr_{1-x}Lu_xMn_2Ge_2$ decreases but is still larger than the first critical value of 2.87 Å for the samples with x=0.2 and 0.4. If we assume that the contraction of the unit cell volume due to Lu substitution (chemical pressure) is equivalent to the influence of external pressure, the corresponding pressures can be derived to be 15.2 kbar and 30.8 kbar for the x=0.2 and 0.4 samples using the Murnaghan equation $p = (B_0 / B_0')[(V / V_0)^{-B_0'} - 1]$ where B_0 is the isothermal bulk modulus, B_0' its pressure derivative and V_0 and V are the volume at ambient pressure and pressure p respectively. In this calculation we used the B_0 (=819 kbar) and B_0' (=4.0) values of $LaMn_2Si_2$ [19] to approximate the values for $PrMn_2Ge_2$.

3.1 Magnetic Properties

$Pr_{0.8}Lu_{0.2}Mn_2Ge_2$: Fig. 2(a) shows the temperature dependence of the magnetization of $Pr_{0.8}Lu_{0.2}Mn_2Ge_2$ as measured in a field of 0.005 T over the temperature range of 5–350 K after cooling in zero field (the warming and cooling curves are marked by arrows). It can be seen clearly that below 350 K two magnetic phase transitions are readily detected at ~ 330 K and ~35 K with indications of a third possible phase transition around ~ 192 K as evidenced by a slight change in

the slope of the M versus T curve (as marked by an arrow; this transition around 192 K is more evident in the dM/dT curve shown as an insert to Fig. 2(a)). DSC measurements (shown as Fig. 2(b)) have been used to check for possible phase transition in the temperature region up to 550 K. Two transitions at around ~ 330 K and ~ 397 K have been detected with the transition at around ~ 330 K agreeing well with the observations from the region of overlap with the magnetisation measurements.

In order to determine the type and order of these transitions, we have measured the field dependence of magnetization (Fig. 3(a)) at selected temperatures and, based on these magnetic data, the Arrot-plot (M^2 versus H/M curves [20]) are drawn in Fig. 3(b). It is clear that, with a positive intercept on the M^2 axis extrapolated from high field, the compound exhibits ferromagnetic character at 300 K, 100 K and 10 K while $Pr_{0.8}Lu_{0.2}Mn_2Ge_2$ behaves like an antiferromagnet or paramagnet at 340 K where a negative intercept on the M^2 axis is obtained.

In comparison with the behaviour of the limiting $PrMn_2Ge_2$ compound which exhibits the antiferromagnetic AFl structure (Fig 1(a)) between 415 K and 334 K and the ferromagnetic F*mc* structure (Fig 1(b)) between 334 K and 280 K [15], it appears reasonable for us to ascribe the transition at ~330 K in $Pr_{0.8}Lu_{0.2}Mn_2Ge_2$ to a transition from the AFl structure to the F*mc* structure while the transition at 35 K can be assumed to be the additional ferromagnetic contribution stemming from ordering of the Pr sublattice at T_C^{Pr}. Likewise, the transition at ~192 K should be assigned to be $T_{c/c}$ from the high temperature canted F*mc* to the lower temperature conical spin structure, F*mi* (Fig 1(c)) while the transition at ~397 K corresponds to the transition from paramagnetism to AFl antiferromagnetism. These conclusions are considered further in discussion of the neutron diffraction results below.

As stated above, as a general guide, if $d^{a}_{Mn\text{-}Mn} > 2.87$ Å, the intralayer in-plane coupling is antiferromagnetic and the interlayer coupling is ferromagnetic [6, 7]. The magnetic behaviour of $Pr_{0.8}Lu_{0.2}Mn_2Ge_2$ can therefore be understood generally in these terms as $d^{a}_{Mn\text{-}Mn}$ at room temperature is 2.893 Å which is larger than the first critical value d_{crit1}~2.87 Å discussed above. Moreover, the values of spontaneous magnetization M_s (and corresponding magnetic moment values per formula unit) have been calculated from the Arrott plot to be: 58.1 emu/g (4.2 μ_B/f.u.), 41.5 emu/g (3.0 μ_B/f.u.) and 26.3 emu/g (1.9 μ_B/f.u.) at 10 K, 100 K and 300 K, respectively.

$Pr_{0.6}Lu_{0.4}Mn_2Ge_2$: Compared with $Pr_{0.8}Lu_{0.2}Mn_2Ge_2$, the value $d^{a}_{Mn\text{-}Mn}$=2.872 Å at room temperature for $Pr_{0.6}Lu_{0.4}Mn_2Ge_2$ is similar to d_{crit1}~2.87 Å. With decreasing temperature, the unit cell will contract and the magnetic interaction between the Mn layers is therefore expected to change from ferromagnetic to antiferromagnetic. Previous investigations [6, 7] of RMn_2Ge_2 indicate that when 2.84 Å < $d^{a}_{Mn\text{-}Mn}$ < 2.87 Å, the intralayer in-plane coupling becomes AF and the interlayer coupling is also AF. In fact, similar to the case of $SmMn_2Ge_2$ [11], re-entrant ferromagnetism of the Mn sublattice [12, 13] has been observed in $Pr_{0.6}Lu_{0.4}Mn_2Ge_2$ below 31 K as shown in the magnetisation data (Fig. 4(a); T_c^{Pr} and T_N^{inter} were determined from the dM/dT versus T curves shown as the inserts to Fig. 4(a)). This ferromagnetic ordering of the Mn sublattice is driven by the ferromagnetic ordering of the Pr sublattice which takes place at T_C^{Pr}=31 K. Likewise [21], as indicated by the magnetisation data of Fig. 4(a) and the DSC data of Fig. 4(b), the transition temperatures have been determined to be ~321 K, ~172 K and ~31 K for T_C^{inter}, T_N^{inter} and T_C^{Pr}, respectively. Fig. 5(a) shows a set of magnetisation versus temperature curves for $Pr_{0.6}Lu_{0.4}Mn_2Ge_2$ at various fields with the field dependence of the critical temperatures T_C^{inter}, T_N^{inter} and T_C^{Pr} shown in Fig. 5(b). As indicated in Fig. 5(b), T_N^{inter} decreases and T_C^{Pr} increases as the magnetic field increases, resulting in a narrowing of the canted AFmc antiferromagnetic range. The field dependence of these magnetic phase transition temperatures is derived to be: $dT_C^{inter}/\mu_0 dH$ = 3.9 K/T; $dT_N^{inter}/\mu_0 dH$ = -8.6 K/T, and $dT_C^{Pr}/\mu_0 dH$ = 3.5 K/T with fitting results shown by the lines in

Fig. 5(b). Similar behaviours have been found in other systems with re-entrant ferromagnetism including: $SmMn_2Ge_2$ [12]; $NdMn_{1.575}Fe_{0.425}Ge_2$ (where $dT_N^{inter}/\mu_0 dH$ = -13 K/T and $dT_C^R/\mu_0 dH$ = 8 K/T) [13]; $PrMn_{0.6}Fe_{0.4}Ge_2$ [21], and $Nd_{0.35}La_{0.65}Mn_2Si_2$ [7]. On the other hand, it was reported that the antiferromagnetic range in $SmMn_2Ge_2$ [14] becomes wider when hydrostatic pressure is applied ($dT_C^R/\mu_0 dH$ = -9.1 K/kbar and $dT_N^{inter}/\mu_0 dH$ = 22.3 K/kbar) [14]. This indicates that the influence of an applied magnetic field on the magnetic phase transitions is opposite to that from external pressure; this behaviour can be understood in terms of the spontaneous magnetovolume effect observed in these systems [7, 21]. Moreover, the transition at T_N^{intra} ~ 375 K from paramagnetism (PM) to ab-plane antiferromagnetism, AFl, has been detected from the DSC measurement for high temperature range (300 K – 550 K) as shown in Fig. 4(b).

The field dependences of the magnetization of $Pr_{0.6}Lu_{0.4}Mn_2Ge_2$ at selected temperature are shown in Fig. 6 (a)) with the corresponding Arrot-plots drawn in Fig. 6(b). These temperatures – 10 K, 100 K, 150 K, and 300 K – were selected as being representative of the different magnetic regions indicated by the magnetisation versus temperature curve of Fig. 4(a). The M^2 versus H/M plots indicate that $Pr_{0.6}Lu_{0.4}Mn_2Ge_2$ exhibits ferromagnetic behaviour at 10 K and 300 K (positive intercepts on the M^2 axis) and antiferromagnetic behaviour at 100 K and 150 K (negative intercepts on the M^2 axis). These findings have been confirmed by our neutron diffraction investigations as discussed in section 3.3 below. Further, in the ferromagnetic regions the M_s and magnetic moment values per formula unit values have been derived to be 38.3 emu/g (2.8 μ_B/f.u.) and 17.2 emu/g (1.3 μ_B/f.u.) at 10 K and 300 K respectively.

Compared with $PrMn_2Ge_2$ (5.28 μ_B/f.u. at 1.5 K), the decrease in M_s at 10 K for $Pr_{0.6}Lu_{0.4}Mn_2Ge_2$ (4.2 μ_B/f.u.) and $Pr_{0.8}Lu_{0.2}Mn_2Ge_2$ (2.8 μ_B/f.u.) can be linked with dilution of the Pr magnetic moment with non magnetic Lu. Assuming that the Mn magnetic moments below T_C^{Pr} are same in these three compounds, M_s is expected to decrease with increase in Lu content as, below the rare

earth ordering temperature T_C^R, the Mn moments order ferromagnetically for light rare earths in RMn_2X_2 compounds (but antiferromagnetically for the heavy rare earths). However, as is well understood, the Mn moment itself is very sensitive to its local environment including the spacing, number and size of neighbouring atoms. As the substitution of Lu for Pr clearly shortens the spacing of the Mn-Mn and Mn-Pr atoms (Table 1), a decrease in the value of the Mn moment due to the decrease of d^a_{Mn-Mn} may also play a role in the overall decrease in M_s with increasing Lu content. Similar effects have been observed in the $GdMn_2Ge_{2-x}Si_x$ system [22] where a decrease in the Mn moment is detected as *x* is increased from 0 to 2.

The magnetisation behaviour exhibited by $Pr_{0.6}Lu_{0.4}Mn_2Ge_2$ in Fig. 4(a) is similar to those of the re-entrant ferromagnetic systems $Nd_{0.35}La_{0.65}Mn_2Si_2$ [22], $Pr_{1-x}Y_xMn_2Ge_2$ [16] and $SmMn_2Ge_2$ [23]. This allows comparison of these related 1-2-2 systems in order to assess the influence of geometrical factors in governing their behaviour. For example, the room temperature lattice parameter of $Pr_{0.6}Lu_{0.4}Mn_2Ge_2$, a = 4.0613 Å, is slightly smaller than that of $Nd_{0.35}La_{0.65}Mn_2Si_2$, a ~ 4.070 Å [22], $Pr_{0.5}Y_{0.5}Mn_2Ge_2$, a = 4.083 Å and $Pr_{0.4}Y_{0.6}Mn_2Ge_2$, a = 4.069 Å [16], but larger than that of $SmMn_2Ge_2$, a ~ 4.045 Å [23]. Moreover, compared with these $R_{1-x}R'_xMn_2Ge_2$ systems, the critical lattice parameters in the $RMn_{2-x}Fe_xGe_2$ system for which re-entrant ferromagnetism is also found to occur, are relatively larger (for example, a = 4.0811 Å in $NdFe_{0.425}Mn_{1.575}Ge_2$ [13] and a = 4.088 Å in $PrMn_{1.4}Fe_{0.6}Ge_2$ [21]). This common re-entrant magnetic behaviour for disparate values of the lattice parameter *a* indicates that geometric factors alone do not govern the magnetic behaviour and that electronic effects also play a role [21].

3.2 Mössbauer Spectroscopy

Typical Mössbauer spectra for the $Pr_{0.8}Lu_{0.2}Mn_2Ge_2$ and $Pr_{0.6}Lu_{0.4}Mn_2Ge_2$ samples at various temperatures between 4.5 K and 300 K are shown in Figs. 7(a) and 8(a) respectively. The ^{57}Fe atoms are expected to predominantly enter the Mn crystallographic 4d site and ideally the spectra

would be fitted using a single sextet to represent ^{57}Fe atoms in the 4d site. In practice, and in agreement with Mössbauer studies of related 1-2-2 compounds, two sextets are generally required to provide the best spectral fits [e.g. 26, 27]. In the present investigation, the fits of the 4.5 K spectra for $Pr_{0.8}Lu_{0.2}Mn_2Ge_2$ and $Pr_{0.6}Lu_{0.4}Mn_2Ge_2$ using one sextet (Figs. 7(b) and 8(b) respectively) are shown for comparison with the fits obtained using two sextets (Figs. 7(a) and 8(a) respectively). These comparisons demonstrate that significant misfits remain when only one sextet is used and highlight the need to include the second sextet for proper representation of the spectra. These two sextets represent ^{57}Fe atoms that predominantly enter the Mn 4d site (sextet I) and those which enter the Ge 4e site (sextet II). The optimal fits to the present spectra reveal that the large majority of ^{57}Fe atoms reside on the 4d site (93(2) % and 96(2) % for $Pr_{0.8}Lu_{0.2}Mn_2Ge_2$ and $Pr_{0.6}Lu_{0.4}Mn_2Ge_2$, respectively) with the remainder of the ^{57}Fe atoms (7(2) % and 4(2) % respectively) residing on the 4e site. This behaviour is also consistent with the fact that sextet I of the Mn 4d site exhibits a larger magnetic hyperfine field than sextet II of the Ge 4e site (e.g. for $Pr_{0.8}Lu_{0.2}Mn_2Ge_2$ at 4.5 K the hyperfine fields are: B_{hf}(4d) = 11.7 T; and B_{hf}(4e) = 5.9 T) [cf. e.g 27]. Examples of the sub-spectral components for $Pr_{0.8}Lu_{0.2}Mn_2Ge_2$ and $Pr_{0.6}Lu_{0.4}Mn_2Ge_2$ are shown in the 4.5 K spectra of Figs. 7(a) and 8(a) respectively.

The temperature dependences of the Mössbauer hyperfine parameters for $Pr_{0.8}Lu_{0.2}Mn_2Ge_2$ and $Pr_{0.6}Lu_{0.4}Mn_2Ge_2$ - as represented by the behaviour of the ^{57}Fe atoms located on the Mn 4d site (sextet I) - are shown in Figs. 9 and 10 respectively. As is well accepted, the observed hyperfine fields result from contributions to the exchange interactions present in the Pr and Mn sublattices and correspondingly reflect the magnetic order in the Pr and Mn sublattices [26-28]. The variation in the hyperfine field values around the transition temperatures determined from the magnetic measurements (Figs 2(a) and 4(a)) is clearly linked with modifications of the magnetic structures. It can be seen from Fig. 9 that, surprisingly, the magnetic hyperfine field for $Pr_{0.8}Lu_{0.2}Mn_2Ge_2$ at 4.5 K (below the ordering temperature for the Pr sublattice of $T_C^{Pr} \sim 35$ K; Fig. 2(a)) is less than the

magnetic hyperfine field at 100 K even though the Pr and Mn moments couple ferromagnetically below T_C^{Pr} as observed in other similar systems such as $NdMn_2Ge_2$ [26]. This implies that the transferred hyperfine field from the rare earth sublattice is opposite to that contributed from the Mn sublattice [21, 26]. For $Pr_{0.6}Lu_{0.4}Mn_2Ge_2$, the transition temperatures T_C^{Pr} and T_N^{inter} are clearly marked by changes in the trends of ^{57}Fe magnetic hyperfine field and the electric quadrupole interaction parameters as shown in Fig. 10. Similar behaviour has been reported in other systems including $PrMn_{2-x}Fe_xGe_2$ [21], $La_{1-x}Y_xMn_2Si_2$ [27] and RMn_2X_2 with X=Ge and Si [26].

The Debye temperatures for $Pr_{0.8}Lu_{0.2}Mn_2Ge_2$ and $Pr_{0.6}Lu_{0.4}Mn_2Ge_2$, have been determined from the temperature dependence of the isomer shift, IS(T) [29, 30]:

$$IS(T) = IS_0(T) + IS_{SODS}(T) \qquad (1)$$

$IS_0(T)$ represents the T dependence of the charge density at the probe nucleus which is generally weakly temperature dependent. The second term, IS_{SODS}, is the so-called second-order Doppler shift, which, using the Debye model for the phonon spectrum, can be described by,

$$IS_{SODS}(T) = -\frac{3kT}{2mc}\left[\frac{3\theta_D}{8T} + 3\left(\frac{T}{\theta_D}\right)^3 \int_0^{\tau} \frac{x^3}{e^x - 1} dx\right], \qquad (2)$$

where m is the mass of the ^{57}Fe nucleus, k Boltzmann's constant, c the velocity of light, and $\tau = \theta_D/T$ the reduced temperature [29, 30]. Debye temperature values of $\theta_D = 320 \pm 20$ K and $\theta_D = 400 \pm 20$ K have been derived for $Pr_{0.8}Lu_{0.2}Mn_2Ge_2$ and $Pr_{0.6}Lu_{0.4}Mn_2Ge_2$ respectively on fitting the mean isomer shift data of Figs 9(c) and 10(c) to equation (2). These Debye temperatures are similar to θ_D values reported for RMn_2X_2 systems. For example, the value of $\theta_D = 338$K has been obtained for YMn_2Ge_2 on fitting the thermal expansion [31], while the value of $\theta_D = 415$ K for $Gd_{1-x}La_xMn_2Ge_2$ and YCo_2Ge_2 has been obtained on fitting the temperature dependence of lattice parameters [32]. In the present case, the tendency for increase in the Debye temperature with increasing Lu content in $Pr_{0.8}Lu_{0.2}Mn_2Ge_2$ and $Pr_{0.6}Lu_{0.4}Mn_2Ge_2$, can be understood in the term of the difference of Debye temperature between Pr ($\theta_D = 85$ K) and Lu ($\theta_D = 185$ K) [33]

3.3 **Neutron Diffraction**

Based on the magnetic regions identified in the magnetisation measurements for $Pr_{0.8}Lu_{0.2}Mn_2Ge_2$ and $Pr_{0.6}Lu_{0.4}Mn_2Ge_2$ (Fig 2(a) and Fig 4(a) respectively), we have measured neutron diffraction patterns for both samples at selected temperatures where different magnetic structures are expected. Figure 11 shows a representative series of neutron diffraction patterns taken for the $Pr_{0.8}Lu_{0.2}Mn_2Ge_2$ compound over the temperature range 5 – 265 K with 10 K temperature steps. As outlined previously [e.g. 15], the special position of the Mn atoms on the 4d sites means that the scattering due to ferromagnetic ordering of the Mn atoms contributes only to reflections obeying the (hkl) conditions h+k=2n and l=2n while the intensity change in the (hkl) reflections with h+k=2n+1 corresponds to the magnetic contribution from the Mn antiferromagnetic ordering within the (001) planes. Moreover, reflections of the type $h + k + l = 2n + 1$ are based on a collinear antiferromagnetic structure between the adjacent Mn planes. Rietveld refinements have been carried out using the FULLPROF program package which allows simultaneous refinement of the structural and magnetic parameters. Typical examples of the Rietveld refinements to neutron diffraction patterns for $Pr_{0.8}Lu_{0.2}Mn_2Ge_2$ and $Pr_{0.6}Lu_{0.4}Mn_2Ge_2$ are shown in Fig 12 and Fig 14 respectively with the refinement results listed in Tables 2 and 3.

$Pr_{0.8}Lu_{0.2}Mn_2Ge_2$: Figs. 12(a), (b), (c) and (d) show neutron diffraction patterns for $Pr_{0.8}Lu_{0.2}Mn_2Ge_2$ at 3 K, 60 K, 220 K and 290 K respectively with the temperature variations of the (112), (101) and $(101)^+$ intensities shown in Fig 13(a). Consistent with the magnetisation results discussed above, the magnetic structure of $Pr_{0.8}Lu_{0.2}Mn_2Ge_2$ at 220 K and 290 K has been determined to be a canted spin structure (Fmc; Fig 1(b)) with the c-axis interlayer spin components aligned parallel and the intralayer components exhibiting antiferromagnetic coupling. As is well known [15], the Fmc magnetic structure in RMn_2Ge_2 systems is characterised by magnetic scattering (in addition to nuclear scattering) at the (101) and (112) peaks. The magnetic scattering

at the (101) peak corresponds to the contribution from antiferromagnetic ordering within the (00*l*) Mn planes while the (112) reflection corresponds to the ferromagnetic component of the Mn moments along the c-axis.

As can be seen in Figs. 12(b) and 12(c), the neutron diffraction patterns of $Pr_{0.8}Lu_{0.2}Mn_2Ge_2$ at 60 K and 3 K feature the satellites peaks $(101)^+$ and $(101)^-$ as well as $(103)^+$ and $(103)^-$. The intensities of these satellites are shown for comparison with the 220 K pattern in Fig. 12(e) (i.e. above the magnetic transition temperature $T_{c/c}$ = 192 K of Fig 2(a)). This satellite behaviour indicates that at 60 K, $Pr_{0.8}Lu_{0.2}Mn_2Ge_2$ exhibits a ferromagnetic mixed incommensurate structure (F*mi*; see Fig. 1(c)) of wavevector (0, 0, q_z). This structure is characterized by the occurrence of satellite peaks of hkl reflections for which (h+k=2n+1) [15]. The behaviour of these magnetic satellite reflections confirms that the transition at $T_{c/c}$ = 192 K revealed in the magnetisation curve of Fig. 2(a), corresponds to a magnetic phase transition from Fmc for T> $T_{c/c}$ = 192 K to Fmi for T< $T_{c/c}$ = 192 K. The component q_z of the wavevector dictates the phase difference between Mn spin along screw axis **c** equal to $2\pi(0, 0, q_z)(0, 0, 1)=2\pi q_z$. The temperature dependence of the propagation vectors q_z has been derived from the Rietveld refinements and is presented in Fig. 13(b) (e.g. q_z = 0.21 at 3 K corresponding to a phase change angle of 76° and a cone semiangle of 52.2° with respect to the c-axis). In addition, the further increase in the intensity of the (112) reflection at 3 K compared with the (112) intensity at 60 K (see Figs 12(e) and 13(a)) can be ascribed to the additional magnetic scattering resulting from magnetic ordering of the Pr-sublattice below T_C^{Pr} = 35 K. The Mn-sublattice moments in $Pr_{0.8}Lu_{0.2}Mn_2Ge_2$ continue to exhibit the Fmi state below T_C^{Pr} = 35 K, which together with the parallel coupling of the Pr-sublattice moments with the Mn moments along the c-axis, results in the region of combined structures (Fmi + F(Pr)) as indicated in Fig. 2(a) and depicted in (Fig 1(d)).

$Pr_{0.6}Lu_{0.4}Mn_2Ge_2$: Comparison of the diffraction patterns for $Pr_{0.6}Lu_{0.4}Mn_2Ge_2$ at 300 K, 100 K and 7 K in Fig. 14, show several significant features. In particular, similar to the discussion for $Pr_{0.8}Lu_{0.2}Mn_2Ge_2$, the behaviour of the (112) and (101) reflections are consistent with ferromagnetic ordering at 300 K of interlayer spin components leading to the Fmc-type magnetic state. We conclude that $Pr_{0.6}Lu_{0.4}Mn_2Ge_2$ exhibits the Fmc structure between T_C^{inter} = 321 K and T_N^{inter} = 172 K as indicated in Fig 4(a). On the other hand the disappearance of the (112) reflection combined with the appearance of the (111) and (113) reflections at 100 K (Fig 14(b)) indicates that the ferromagnetic ordering at 300 K of interlayer spin components has given way to antiferromagnetic coupling at 100 K, resulting in the AFmc structure depicted in Fig 1(e) [7, 15]. Based on our magnetisation and neutron diffraction results we therefore conclude that $Pr_{0.6}Lu_{0.4}Mn_2Ge_2$ exhibits the AFmc structure between T_N^{inter} = 172 K and T_C^{Pr} = 31 K as indicated in Fig 4(a). The absence of magnetic scattering from the (111) and (113) reflections at 7 K, combined with the increase of the (112) and (101) peak intensities (Fig 14(a)), indicates that the interlayer spin components of the Mn moments align parallel, again leading to an Fmc structure for the Mn-sublattice. In noting the increased magnetisation below T_C^{Pr} = 31 K as in Fig. 4(a), the additional contributions from Pr moments coupled parallel to the Mn moments along the c-axis lead to the combined (Fmc+F(Pr))-type magnetic structure ((Fig 1(f)) for $Pr_{0.6}Lu_{0.4}Mn_2Ge_2$ below T_C^{Pr} = 31 K. It should be noted that with the limited resolution of the MPRD data no evidence for satellite reflections, indicative of the Fmi structure, were observed in Fig 14. The absence of the Fmi structure in $Pr_{0.6}Lu_{0.4}Mn_2Ge_2$ is consistent with the behaviour of the $PrMn_2Ge_2$ (q_z =0.28 at 2 K) and $Pr_{0.8}Lu_{0.2}Mn_2Ge_2$ (q_z =0.21 at 3 K) compounds which demonstrate that q_z decreases with Lu substitution.

While it was not possible to obtain neutron diffraction patterns above room temperature for both samples, as mentioned above, we can none the less conclude that $Pr_{0.8}Lu_{0.2}Mn_2Ge_2$ and $Pr_{0.6}Lu_{0.4}Mn_2Ge_2$ exhibit the antiferromagnetic AFl structure ((Fig 1(a)) between 330-397 K (Fig. 2(b)) and 321-375 K (Fig. 4(b) respectively. This conclusion is based on the analogues between

$Pr_{0.8}Lu_{0.2}Mn_2Ge_2$ and $PrMn_2Ge_2$ [15, 26] as well as between $SmMn_2Ge_2$ [11-13] and $Pr_{0.6}Lu_{0.4}Mn_2Ge_2$ which both exhibit similar magnetic behaviours and the presence of the AFl state above T_C^{Inter}. Overall, combined with the magnetisation results outlined above, the neutron investigations have enabled the magnetic structures of $Pr_{0.8}Lu_{0.2}Mn_2Ge_2$ and $Pr_{0.6}Lu_{0.4}Mn_2Ge_2$ to be determined. The magnetic regions and their magnetic structures are summarised in Figs 2 and 4.

4. Conclusions

The magnetic phase transitions in $Pr_{1-x}Lu_xMn_2Ge_2$ (x=0.2, x=0.4) has been investigated and their magnetic structures determined. $Pr_{0.8}Lu_{0.2}Mn_2Ge_2$ displays antiferromagnetism below Néel temperature T_N^{intra} = 397 K transforming to three successive ferromagnetic phases below T_N^{inter} = 300 K, with ferromagnetic order of the Pr sublattice also occurring below T_C^{Pr} = 35 K (Fig 2). $Pr_{0.6}Lu_{0.4}Mn_2Ge_2$ also displays antiferromagnetism below T_N^{intra} = 375 K, with decrease in temperature leading to successive ferromagnetic, antiferromagnetic and ferromagnetic phases and the re-entrant ferromagnetic behaviour shown in Fig 4. Ferromagnetic order of the Pr sublattice also occurs below T_C^{Pr} = 31 K.

Substitution of Lu for Pr decreases the spacing of the Mn-Mn and Mn-Pr atoms (Table 1), leading to a decrease of Mn moment itself at 4.5 K in addition to the dilution effect of Pr moment. The Debye temperatures have been derived to be 320 K and 400 K for $Pr_{0.8}Lu_{0.2}Mn_2Ge_2$ and $Pr_{0.6}Lu_{0.4}Mn_2Ge_2$, respectively. Below the Pr ordering temperature, T_C^{Pr}, the transferred hyperfine fields at the ^{57}Fe nucleus in both $Pr_{0.8}Lu_{0.2}Mn_2Ge_2$ and $Pr_{0.6}Lu_{0.4}Mn_2Ge_2$ are found to be smaller at 4.5 K than above T_C^{Pr} (Figs 9(a) and 10(a)), thus establishing that the transferred hyperfine field from Pr is opposite to that produced by Mn. The magnetic structures for $Pr_{0.8}Lu_{0.2}Mn_2Ge_2$ and $Pr_{0.6}Lu_{0.4}Mn_2Ge_2$ are summarised in Figs 2 and 4 respectively with the relevant magnetic structures depicted in Fig 1.

Acknowledgements

The authors would like to acknowledge the contributions which Dr Trevor Hicks of Monash University has made throughout his career to the advancement of neutron science and studies of magnetism in Australia. SJC in particular acknowledges the contributions which Dr Hicks made as supervisor during his PhD studies. The work is also supported in part by grants from the Australian Institute of Nuclear Science and Engineering, the Australian Research Council Discovery Grant (DP0879070) and the Australian Research Council LIEF Grant (LE0775559).

Reference:

[1] T. Fujiwara, H. Fujii H, T. Shigeoka, Phys. Rev. B **63**, 174440 (2001)

[2] S. Chaudhary, M.K. Chattopadhyay, K.J. Singh, S.B. Roy, P. Chaddah, E.V. Sampathkumaran, Phys. Rev. B **66**, 014424 (2002)

[3] M. Hofmann, S.J. Campbell and A.V.J. Edge, Phys. Rev. B **69**, 174432 (2004)

[4] A. M. Bebb, J. W. Taylor, J. A. Duffy, Z. F. Banfield, M. J. Cooper, M. R. Lees, J. E. McCarthy and D. N. Timms, Phys. Rev. B **71**, 024407 (2005)

[5] E.G. Gerasimov, N.V. Mushnikov and T. Goto, Phys. Rev. B **72**, 064446 (2005)

[6] Szytula A and Leciejewicz J 1994 Handbook on Crystal Structures and Magnetic Properties of Rare Earth Intermetallics (Boca Raton, FL: CRC Press)

[7] G. Venturini, B. Malaman and E. Ressouche, J. Alloys Compounds **240**, 139 (1996); G. Venturini, R. Welter, E. Ressouche and B. Malaman, J. Magn. Magn. Mater. **150,** 197 (1995) and references therein; J. S. Lord, P. C. Riedi, G. J. Tomka, Cz. Kapusta and K. H. J. Buschow, Phys. Rev. B **53**, 283 (1995).

[8] V. K. Pecharsky and K. A. Gschneidner, Jr, Phys. Rev. Lett., **78,** 4494 (1997).

[9] R. Nirmala and S. K. Malik, Europhys**.** Lett. **80**, 27001 (2007)

[10] M.H. Phan and S.C. Yu, J. Magn. Magn. Mater. **308**, 325 (2007)

[11] H. Fujii, T. Okamoto, T. Shigeoka, and N. Iwata, Solid State Commun. **53**, 715 (1985)

[12] M. Duraj, R. Duraj, A. Szytula and Z. Tomkowicz, J. Magn. Magn. Mater. **73,** 240 (1988)

[13] G. Venturini, B. Malaman and E. Ressouche, J. Alloy. Comp. **237**, 61 (1996)

[14] P. Kumar, K.G. Suresh, A.K. Nigam, A. Magnus, A.A. Coelho and S. Gama, Phys. Rev. B **77**, 224427 (2008)

[15] Welter R, Venturini G, Ressouche E and Malaman B J. Alloys Compounds **218,** 204 (1995)

[16] Y.G. Wang, F.M. Yang, C.P. Chen, N. Tang and Q.D. Wang, J. Phys.: Condens. Matter **9**, 8539 (1997)

[17] J.L. Wang, N. Tang, Y.P. Shen, D. Yang, B. Fuquan, G.H. Wu, F.M. Yang, F.R. de Boer, E. Bruck and K.H.J. Buschow, J. Appl. Phys. **91,** 2165 (2002); J.L. Wang**,** C. Marquina, M.R. Ibarra and G.H. Wu, Phys. Rev. B **73**, 094436 (2006); J. L. Wang, S. J. Campbell, O. Tegus, C. Marquina and M. R. Ibarra, Phys. Rev. B **75,** 174423 (2007)

[18] L. Gelato, J. Appl. Crystallogr. **14**, 151 (1981)

[19] M. Hofmann, S.J. Campbell, K. Knorr, S. Hull and V. Ksenofontov, J. Appl. Phys. **91**, 8126 (2002)

[20] A. Arrott, Phys. Rev. **108**, 1394 (1957)

[21] J.L. Wang, S.J. Campbell, J.M. Cadogan, O. Tegus, A J Studer and M Hofmann, J. Phys.: Condens. Matter **18**, 189 (2006); J.L. Wang, A J Studer, S.J. Campbell, M Hofmann and J.M. Cadogan, Physica B **385-386**, 326 (2006).

[22] P. Kumar, N.K. Singh, K.G. Suresh, A.K. Nigam and S.K. Malik, J. Appl. Phys. **101**, 013908 (2007)

[23] G.J. Tomka, C. Ritter, P.C. Riedi, C. Kapusta and W. Kocemba, Phys. Rev. B **58,** 6330 (1998)

[24] T. Kawashima, T. Kanomata, H. Yoshida and T. Kaneko, J. Magn. Magn. Mater. **90-91**, 721 (1990)

[25] G.J. Tomka, C. Ritter, P.C. Riedi, Cz. Kapusta and W. Kocemba, Phys. Rev. B **58**, 6330 (1998)

[26] I. Nowik, Y. Levi, I. Felner and E.R. Bauminger, J. Magn. Magn. Mater. **147,** 373 (1995)

[27] H.S. Li, J.M. Cadogan, X.L. Zhao and S.J. Campbell, Hyperfine Interact. **94,** 1943 (1994); H.S. Li, J.M. Cadogan, X.L. Zhao and S.J. Campbell, J. Magn. Magn. Mater. **147,** 91 (1995); S.J. Campbell, J.M. Cadogan, X.L. Zhao, M. Hofmann and H.S. Li, J. Phys.: Condens. Matter **11**, 7835 (1999)

[28] I. Nowik, I. Felner and E.R. Bauminger, Phys. Rev. B **55**, 3033 (1997)

[29] J. Cieślak, S. M. Dubiel, J. Źukrowski, M. Reissner and W. Steiner, Phys. Rev. B **65**, 212301 (2002)

[30] G.J. Long, D. Hautot, F. Grandjean, D.T. Morelli and G.P. Meisner, Phys. Rev. B **60**, 7410 (1999)

[31] J.H.V.J. Brabers, A.J. Nolten, F. Kayzel, S.H.J. Lenczowski, K.H.J. Buschow, F.R. de Boer, Phys. Rev. B **50**, 16410 (1994)

[32] G.H. Guo, R.Z. Levitin, A. Yu. Sokolov, V.V. Snegirev, D.A. Filippov, J. Magn. Magn. Mater. **214**, 301 (2000)

[33] D. Singth and Y.P. Varshni, Phys. Rev. B **15**, 4340 (1981) and reference therein

Figure captions

Fig. 1 The magnetic structures relevant to discussion of the RMn_2X_2 compounds (R atoms – larger light circles; Ge atoms – larger dark circles; Mn atoms - small circles). The different structure types are defined in [7].

Fig. 2 (a) The temperature dependence of magnetisation for $Pr_{0.8}Lu_{0.2}Mn_2Ge_2$ over the range 3 – 350 K as measured in a magnetic field of 0.005 T on warming (W) after first zero field cooling (ZFC). Measurements were then obtained in a magnetic field of 0.005 T on cooling (C). The insert to Fig. 2(a) shows the dM/dT versus T curve indicating how $T_{c/c}$ was determined.

(b) DSC measurements for $Pr_{0.8}Lu_{0.2}Mn_2Ge_2$ over the temperature range 300 – 550 K.

Fig. 3(a) The variation of magnetization with applied magnetic field (H_{appl} = 0–50 kOe) for $Pr_{0.8}Lu_{0.2}Mn_2Ge_2$ at the temperatures indicated.

(b) The Arrot-plots (M^2 versus M/H) derived from the magnetisation data of Fig 3(a).

Fig. 4 (a) The temperature dependence of magnetisation for $Pr_{0.6}Lu_{0.4}Mn_2Ge_2$ as measured in a magnetic field of 0.005 T on warming after zero field cooling (ZFC). The inserts to Fig. 4(a) show the dM/dT versus T curves indicating how T_C^{Pr} and T_N^{inter} were determined.

(b) DSC measurements over the temperature range 300 – 550 K.

Fig. 5(a) The temperature dependence of magnetisation for $Pr_{0.6}Lu_{0.4}Mn_2Ge_2$ at the magnetic field values indicated, and

(b) a partial magnetic phase diagram for $Pr_{0.6}Lu_{0.4}Mn_2Ge_2$. The dashed lines represent fits to the data as described in the text.

Fig. 6(a) The variation of magnetization with applied magnetic field (H_{appl} = 0–50 kOe) for $Pr_{0.6}Lu_{0.4}Mn_2Ge_2$ at the temperatures indicated and

(b) the Arrot-plots (M^2 versus M/H) derived from the magnetisation data of Fig 6(a).

Fig. 7(a) ^{57}Fe Mössbauer spectra of $Pr_{0.8}Lu_{0.2}Mn_2Ge_2$ over the temperature range 4.5 - 300 K. The spectra were fitted using two sextets. The sub spectral component (sextet II; dashed line in the 4.5 K spectrum) indicates the fraction (~7(2) %) of ^{57}Fe atoms located in the Ge 4e site as discussed in the text. The remainder of the ^{57}Fe atoms (sextet I; ~93(2) %) are located in the Mn 4d site.

(b) ^{57}Fe Mössbauer spectrum of $Pr_{0.8}Lu_{0.2}Mn_2Ge_2$ at 4.5 K fitted using one sextet.

Fig. 8(a) ^{57}Fe Mössbauer spectra of $Pr_{0.6}Lu_{0.4}Mn_2Ge_2$ over the temperature range 4.5 - 300 K. The spectra were fitted using two sextets. The sub spectral component (sextet II; dashed line in 4.2 K spectrum) indicates the fraction (~4(2) %) of ^{57}Fe atoms located in the Ge 4e site as discussed in the text. The remainder of the ^{57}Fe atoms (sextet I; ~96(2) %) are located in the Mn 4d site.

(b) ^{57}Fe Mössbauer spectrum of $Pr_{0.6}Lu_{0.4}Mn_2Ge_2$ at 4.5 K fitted using one sextet.

Fig. 9 Temperature dependences of the Mössbauer hyperfine parameters (sextet I) of $Pr_{0.8}Lu_{0.2}Mn_2Ge_2$:

(a) average magnetic hyperfine field B_{hf};

(b) quadrupole shift ε

(c) isomer shift δ.

The line in Fig 9(c) represents the fit of the isomer shift data to equation (2) resulting in the Debye temperature θ_D = 320 ± 20 K. The dashed lines in Figs 9(a) and (b) represent the trends of the data.

Fig. 10 Temperature dependences of the Mössbauer hyperfine parameters (sextet I) of $Pr_{0.6}Lu_{0.4}Mn_2Ge_2$:

(a) average magnetic hyperfine field B_{hf};

(b) quadrupole shift ε

(c) isomer shift δ.

The line in Fig 10(c) represents the fit of the isomer shift data to equation (2) resulting in the Debye temperature θ_D = 400 ± 20 K. The dashed and full lines in Fig 10(a) and the dashed line in Fig 10 (b) represent the trends of the data.

Fig. 11 Representative neutron diffraction patterns for $Pr_{0.8}Lu_{0.2}Mn_2Ge_2$ over the temperature range 5 - 265 K at 10 K intervals as obtained on the high intensity diffractometer Wombat, OPAL (λ = 2.410 Å).

Fig. 12 (a), (b), (c), (d) Plots of Rietveld refinements to the neutron diffraction patterns for $Pr_{0.8}Lu_{0.2}Mn_2Ge_2$ at 3 K, 60 K, 220 K, 290 K respectively (λ = 2.410 Å; Wombat, OPAL). The lines show the calculated profiles through the experimental data and the residuals. The markers for the crystallographic (top) and magnetic (bottom) structures are indicated for the 3 K pattern in Fig 12(a).

Figure (e) shows expanded 2θ ranges for the 3 K, 60 K and 220 K patterns.

Fig. 13 Temperature dependences of:

(a) the (101), (112) and $(101)^+$ peak intensities and

(b) the q_z component of the wavevector for $Pr_{0.8}Lu_{0.2}Mn_2Ge_2$ as discussed in the text.

Fig. 14 (a), (b), (c) Plots of Rietveld refinements to the neutron diffraction patterns of $Pr_{0.6}Lu_{0.4}Mn_2Ge_2$ at 7 K, 100 K and 300 K respectively (λ = 1.6660 Å; MRPD, HIFAR). The lines show the calculated profiles through the experimental data and the residuals. The markers for the crystallographic (top) and magnetic (bottom) structures are indicated for the 7 K pattern in Fig 14(a).

Figs. (d) and (e) show 2θ regions of interest at 7 K, 100 K and 300 K on expanded scales for several peaks with magnetic scattering .

Table 1 Lattice parameters and structural information for the $Pr_{1-x}Lu_xMn_2Ge_2$ compounds at room temperature (the errors for the lattice parameters *a* and *c*, and the interatomic spacing distances were derived to be ± 0.001 Å from the data fits; z_{Ge}: ± 0.001). $\Delta V/V_0=(V-V_0)/V_0$ where V and V_0 are the volume are the unit cell volume for $Pr_{1-x}Lu_xMn_2Ge_2$ and $PrMn_2Ge_2$, respectively

x	d_{Mn-Mn} (Å)	d_{Mn-Ge} (Å)	d_{Mn-Pr} (Å)	d_{Pr-Ge} (Å)	d_{Pr-Pr} (Å)	d_{Ge-Ge} (Å)	*a* (Å)	*c* (Å)	*V* (Å^3)	z	$\Delta V/V_0$ (%)	[Ref]
0	2.915	2.510	3.422	3.192	4.123	2.600	4.123	10.925	185.7	0.381		[15]
0.2	2.893	2.511	3.407	3.158	4.091	2.537	4.091	10.898	182.4	0.384	1.78	
0.4	2.872	2.497	3.393	3.138	4.061	2.497	4.061	10.873	179.3	0.385	3.45	
1.0	2.785				3.939		3.939	10.809	167.7		9.69	[7]

Table 2 Structural and magnetic parameters derived from Rietveld refinements of the neutron diffraction patterns for $Pr_{0.8}Lu_{0.2}Mn_2Ge_2$ compound (*cf.* Fig 12). The errors were derived from the data fits (the errors are shown for the 3 K data).

T (K)	3 K	60 K	220 K	290 K
a (Å)	4.0726(3)	4.0734(3)	4.0810(4)	4.0852(5)
c (Å)	10.8589(14)	10.8589(14)	10.8748(18)	10.8869(20)
z_{Ge}	0.3823(3)	0.3828(2)	0.381(3)	0.3814(4)
μ_{ab} (μ_B)	2.71(7)	2.68(6)	1.09(3)	1.04(3)
μ_Z (μ_B)	2.10(7)	2.07(6)	1.36(1)	1.36(1)
μ_{total} (μ_B)	3.43(7)	3.38(6)	1.74 (2)	1.71(2)
q_z	0.215(2)	0.196(2)		
μ_{Pr} (μ_B)	3.13 (9)	-	-	
R_{wp}	6.41	6.35	7.26	7.14
R_{exp}	1.52	1.51	1.53	1.54

Table 3 Structural and magnetic parameters derived from Rietveld refinement of neutron diffraction patterns at selected temperatures for $Pr_{0.6}Lu_{0.4}Mn_2Ge_2$ (*cf.* Fig 14). The errors were derived from the data fits (the errors are shown for the 3 K data).

T (K)	7 K	100 K	300 K
a (Å)	4.0514(13)	4.0468(15)	4.0673(1)
c (Å)	10.8499(39)	10.8563(43)	10.8838(26)
z_{Ge}	0.3832(7)	0.383(1)	0.382(1)
μ_{ab} (μ_B)	2.03 (5)	1.65(15)	1.54(11)
μ_Z (μ_B)	2.12 (7)	1.26(26)	1.31(24)
μ_{total} (μ_B)	2.94(9)	2.08(20)	2.02 (19)
μ_{Pr} (μ_B)	1.98(9)	-	-
R_{wp}	1.98	2.09	2.79
R_{exp}	3.70	3.55	4.62

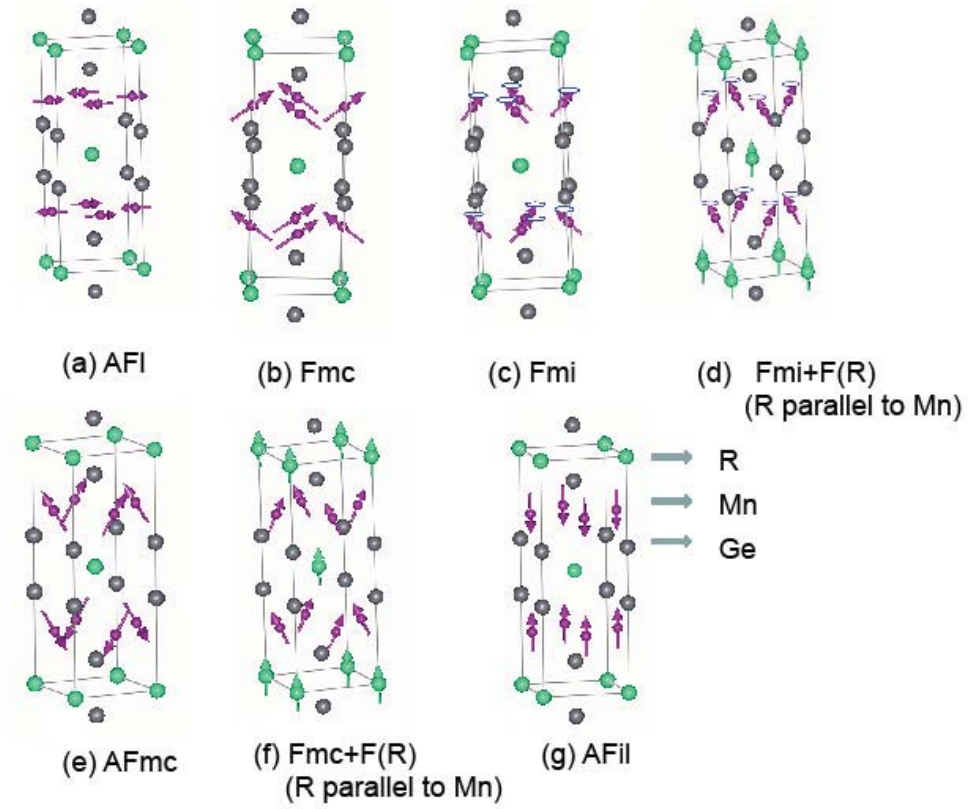
(a) AFI
(b) Fmc
(c) Fmi
(d) Fmi+F(R)
(R parallel to Mn)
(e) AFmc
(f) Fmc+F(R)
(R parallel to Mn)
(g) AFil
R
Mn
Ge

Fig. 1

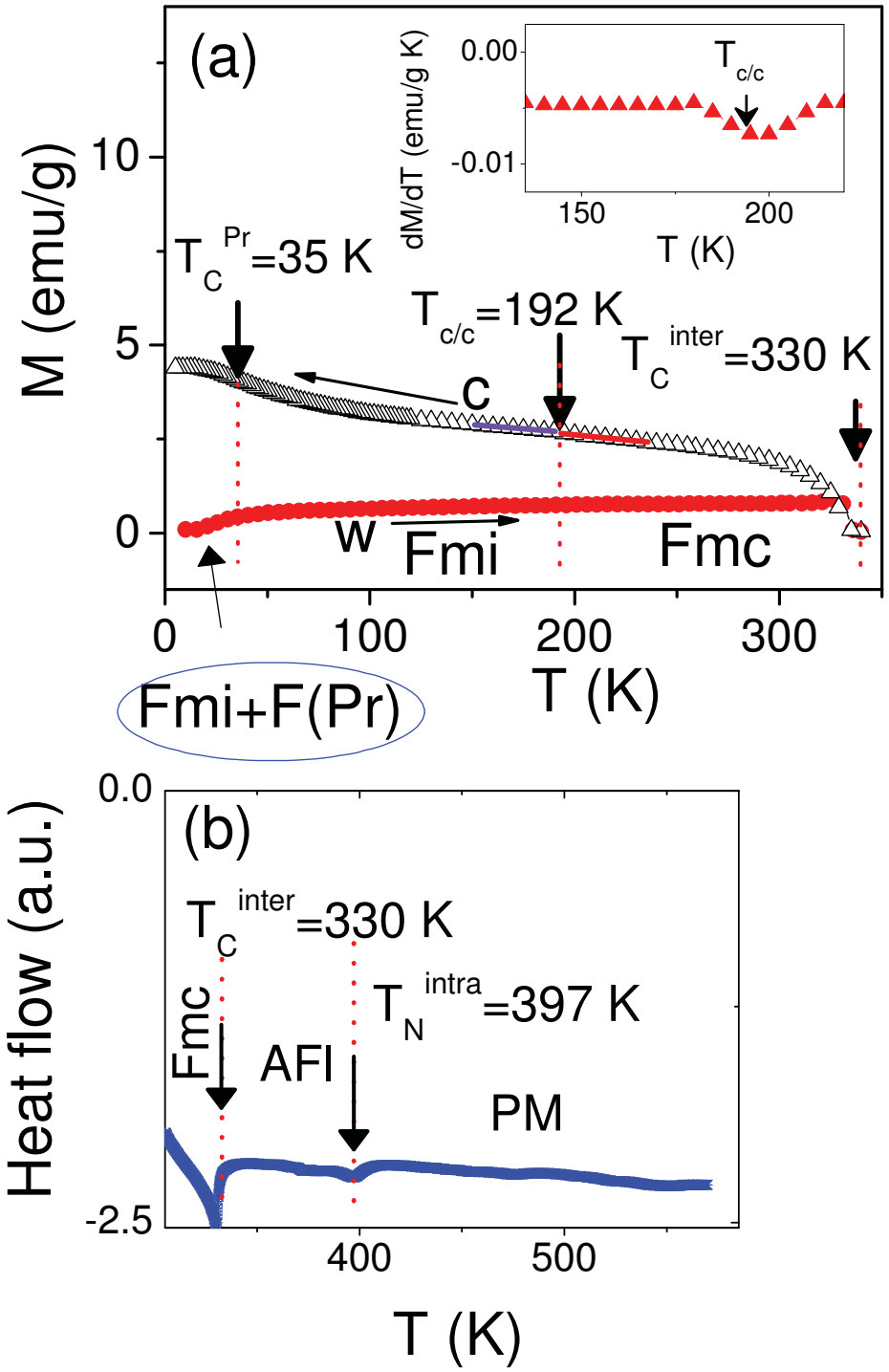
(a)
M (emu/g)
10
5
0
0
100
200
300
T (K)
dM/dT (emu/g K)
0.00
-0.01
150
200
T (K)
T_c/c
T_C^Pr=35 K
T_c/c=192 K
T_C^inter=330 K
c
w
Fmi
Fmc
Fmi+F(Pr)
(b)
Heat flow (a.u.)
0.0
-2.5
400
500
T (K)
T_C^inter=330 K
T_N^intra=397 K
Fmc
AFI
PM

Fig. 2

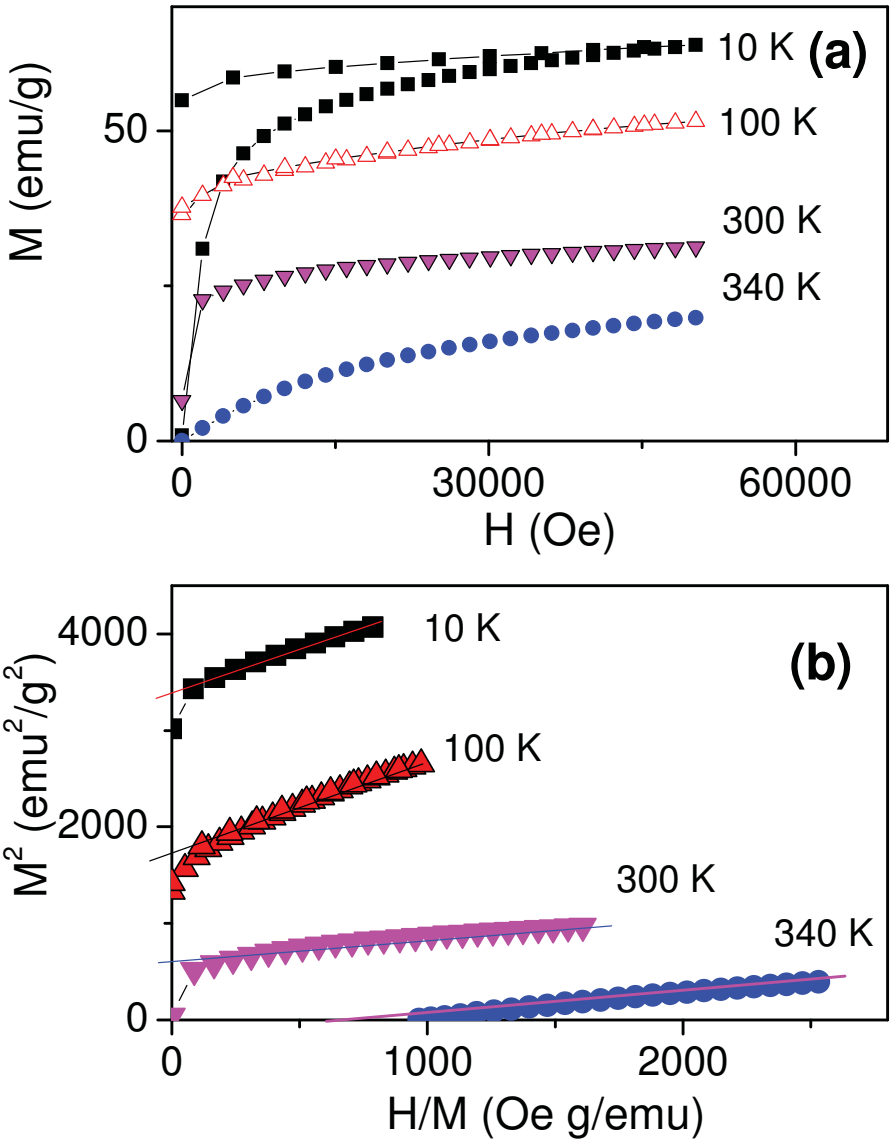
M (emu/g)
50
0
0
30000
60000
H (Oe)
10 K
(a)
100 K
300 K
340 K
M2 (emu2/g2)
4000
2000
0
0
1000
2000
H/M (Oe g/emu)
10 K
(b)
100 K
300 K
340 K

Fig. 3

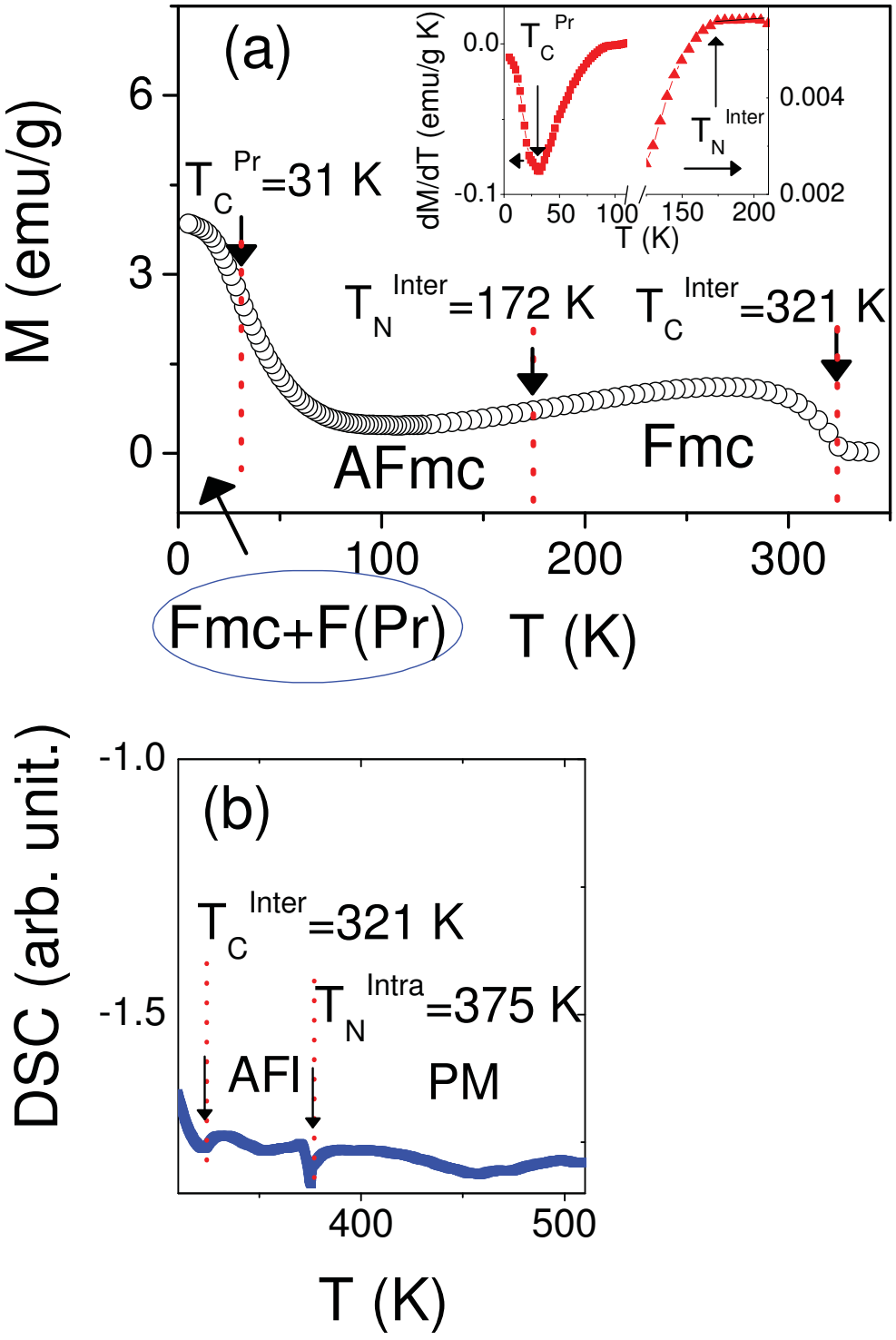
(a)
M (emu/g)
6
3
0
0
100
200
300
T (K)
T_C^{Pr}=31 K
T_N^{Inter}=172 K
T_C^{Inter}=321 K
AFmc
Fmc
Fmc+F(Pr)
dM/dT (emu/g K)
0.0
-0.1
0.004
0.002
0
50
100
150
200
T (K)
T_C^{Pr}
T_N^{Inter}
(b)
DSC (arb. unit.)
-1.0
-1.5
T_C^{Inter}=321 K
T_N^{Intra}=375 K
AFI
PM
400
500
T (K)

Fig. 4

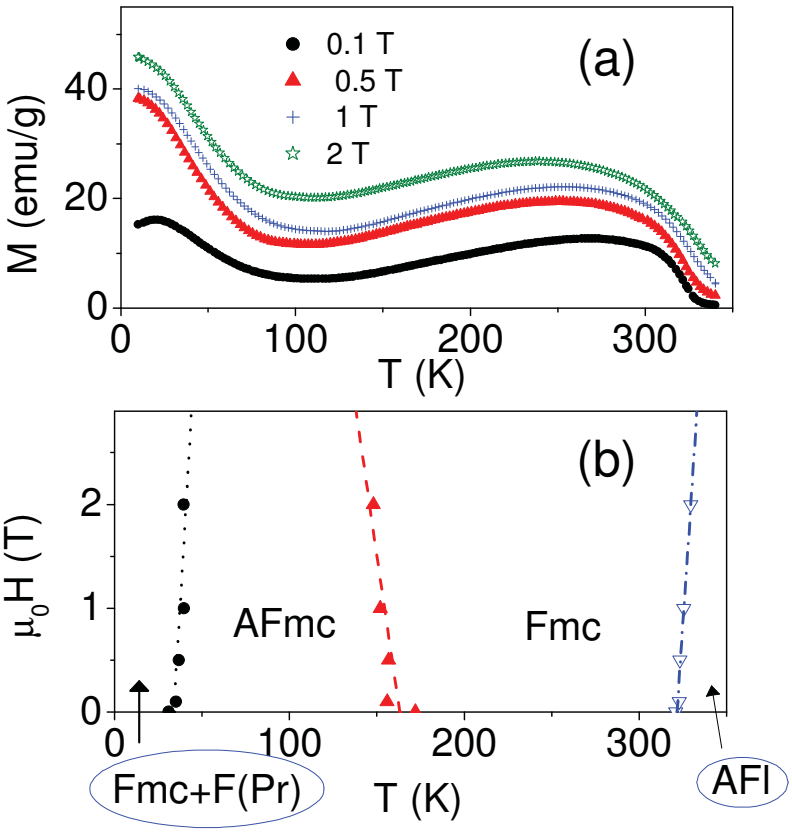

Fig. 5

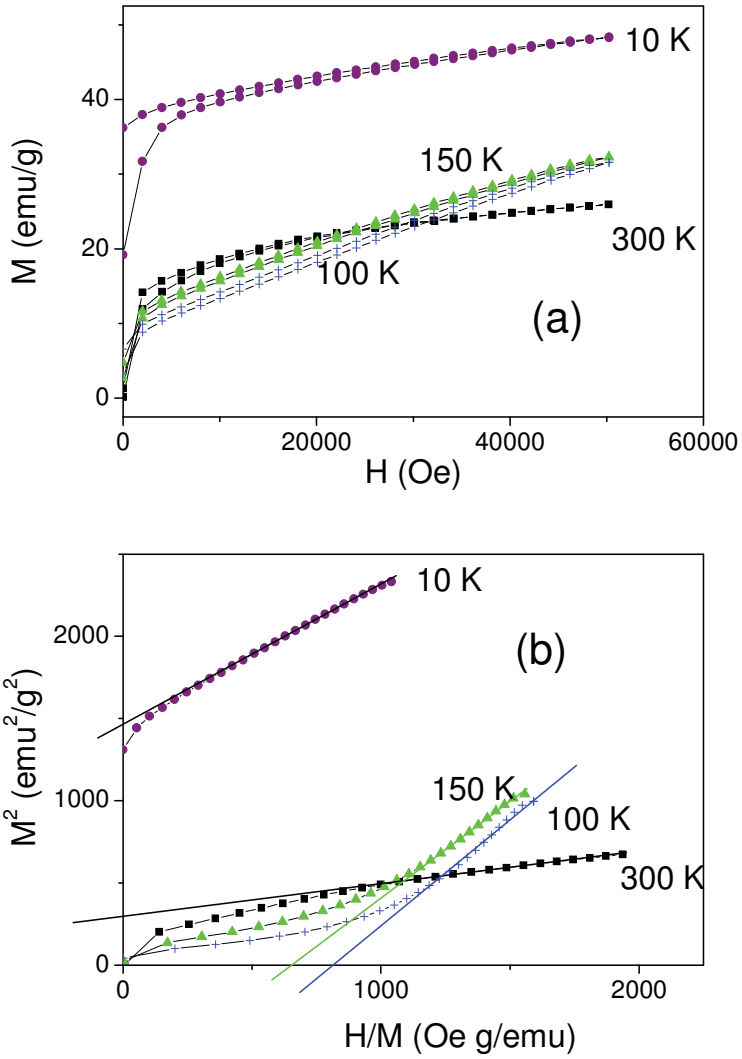
10 K
150 K
300 K
100 K
(a)
M (emu/g)
H (Oe)
0
20
40
0
20000
40000
60000
10 K
(b)
150 K
100 K
300 K
M² (emu²/g²)
H/M (Oe g/emu)
0
1000
2000
0
1000
2000

Fig. 6

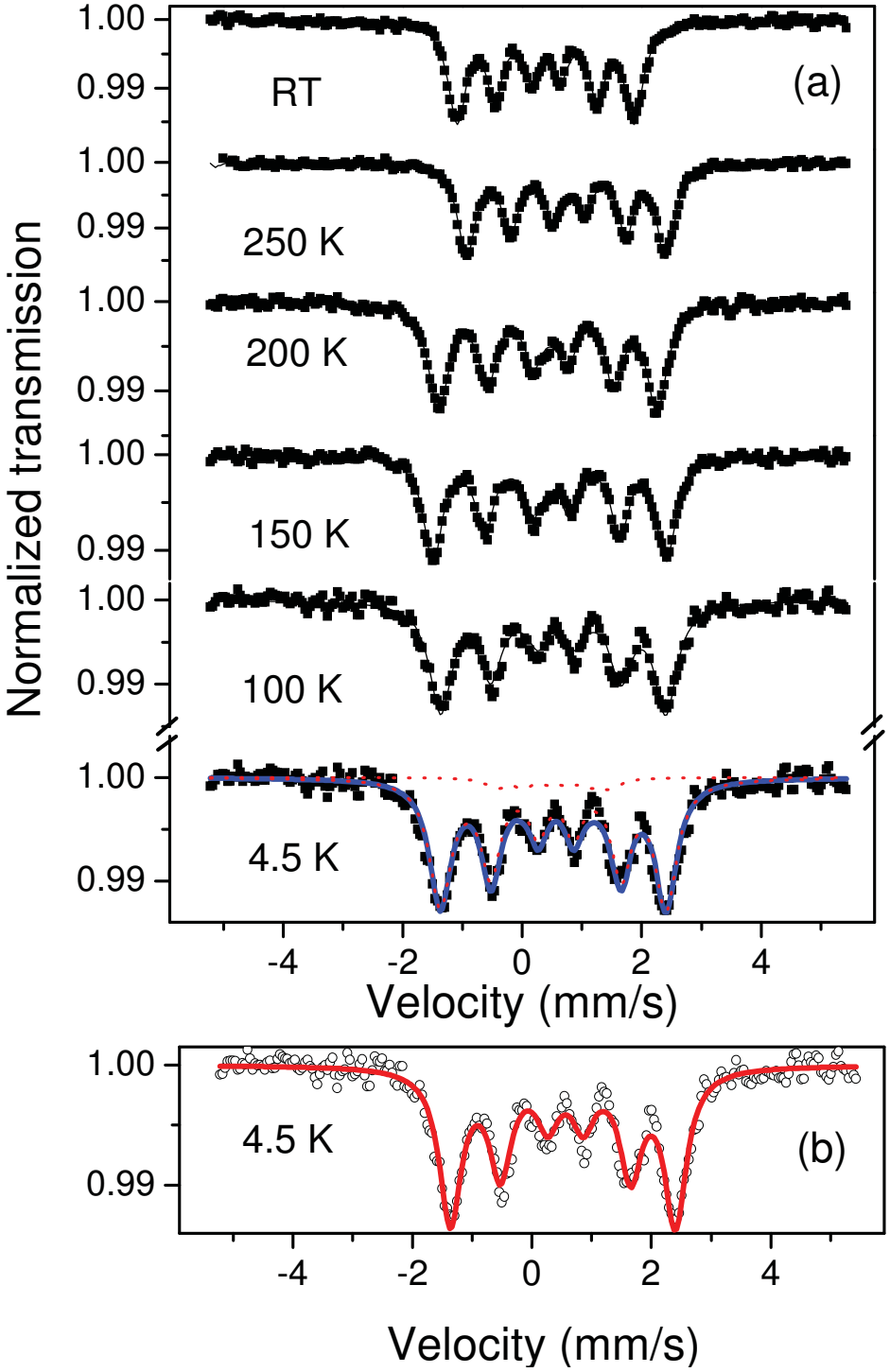
Normalized transmission
1.00
0.99
RT
(a)
250 K
200 K
150 K
100 K
4.5 K
-4
-2
0
2
4
Velocity (mm/s)
4.5 K
(b)
Velocity (mm/s)

Fig. 7

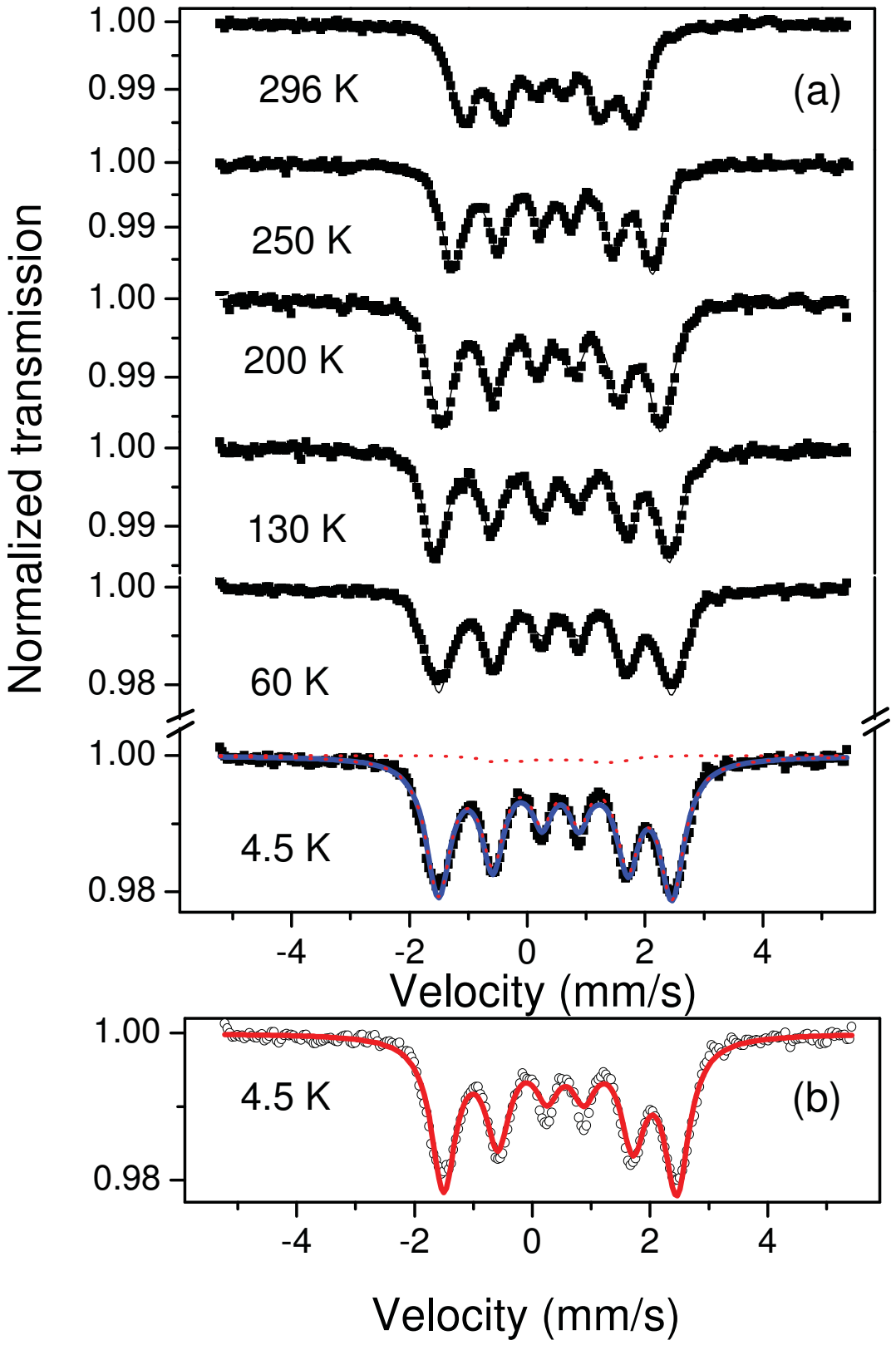
Normalized transmission
1.00
0.99
296 K
(a)
1.00
0.99
250 K
1.00
0.99
200 K
1.00
0.99
130 K
1.00
0.98
60 K
1.00
0.98
4.5 K
-4
-2
0
2
4
Velocity (mm/s)
1.00
0.98
4.5 K
(b)
-4
-2
0
2
4
Velocity (mm/s)

Fig. 8

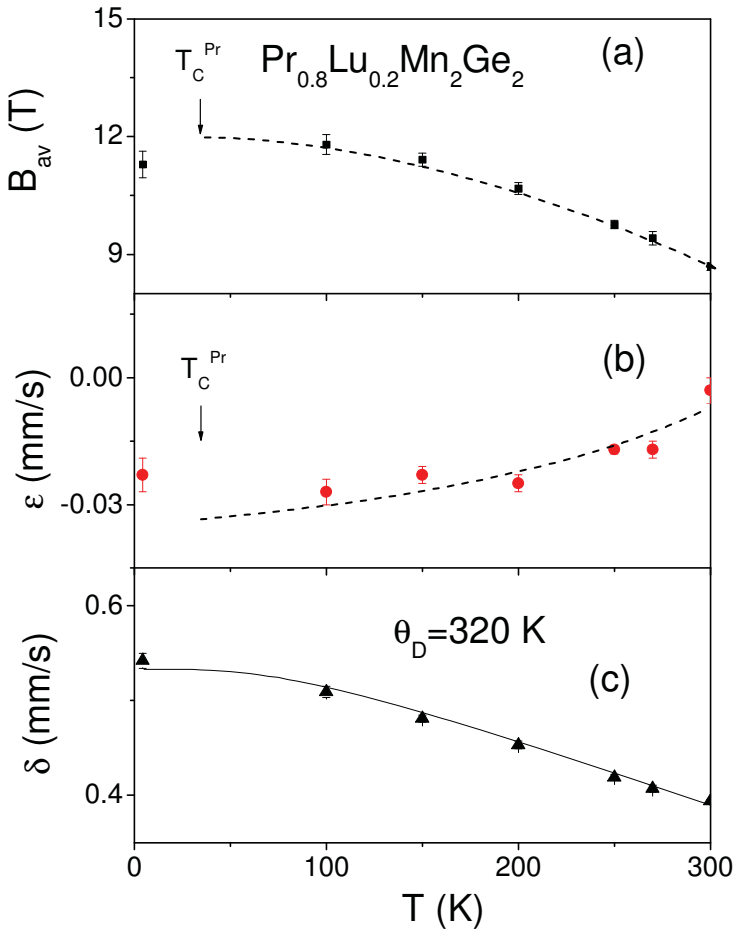
15
12
9
B_av (T)
T_C^Pr
Pr0.8Lu0.2Mn2Ge2
(a)
0.00
-0.03
ε (mm/s)
T_C^Pr
(b)
0.6
0.4
δ (mm/s)
θD=320 K
(c)
0
100
200
300
T (K)

Fig. 9

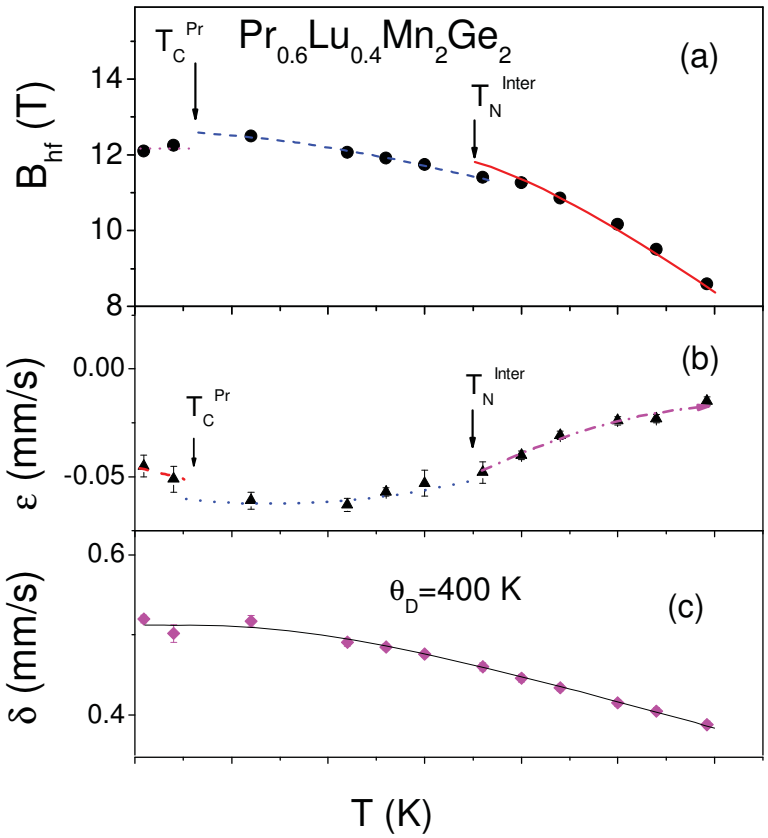
T_C^{Pr}
$Pr_{0.6}Lu_{0.4}Mn_2Ge_2$
(a)
T_N^{Inter}
B_{hf} (T)
14
12
10
8
(b)
0.00
-0.05
ε (mm/s)
δ (mm/s)
0.6
0.4
θ_D=400 K
(c)
T (K)

Fig. 10

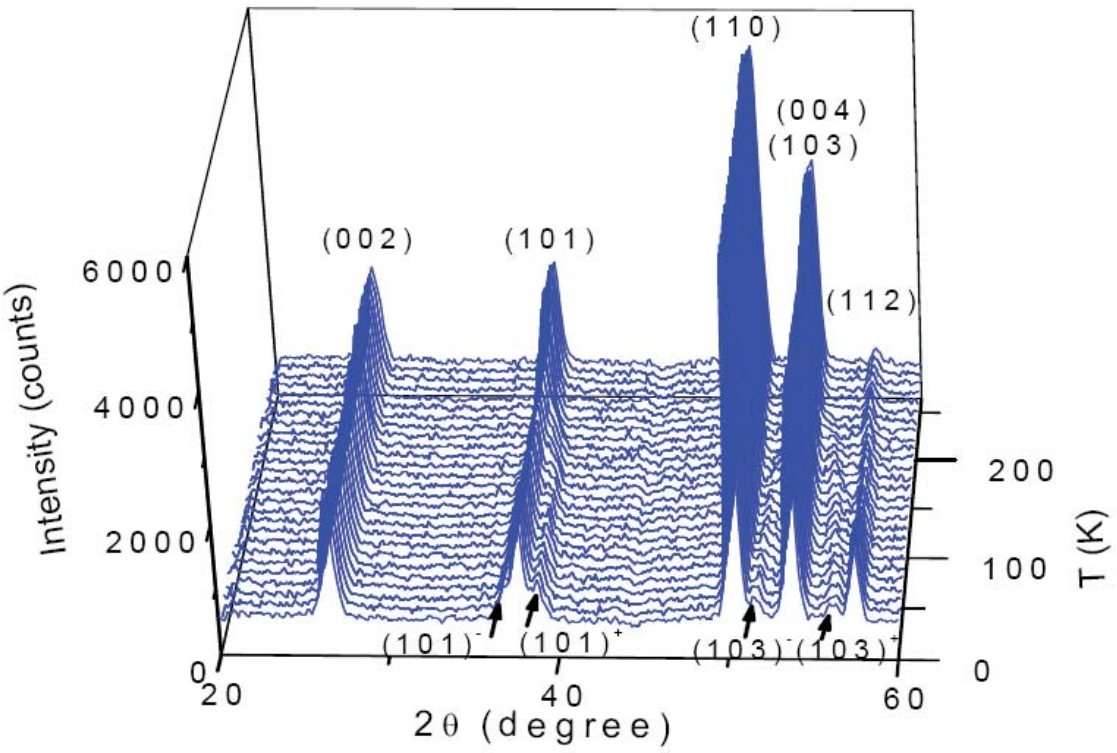
(110)
(004)
(103)
(002)
(101)
(112)
6000
4000
2000
0
Intensity (counts)
20
40
60
2θ (degree)
200
100
0
T (K)
(101)⁻
(101)⁺
(103)⁻
(103)⁺

Fig. 11

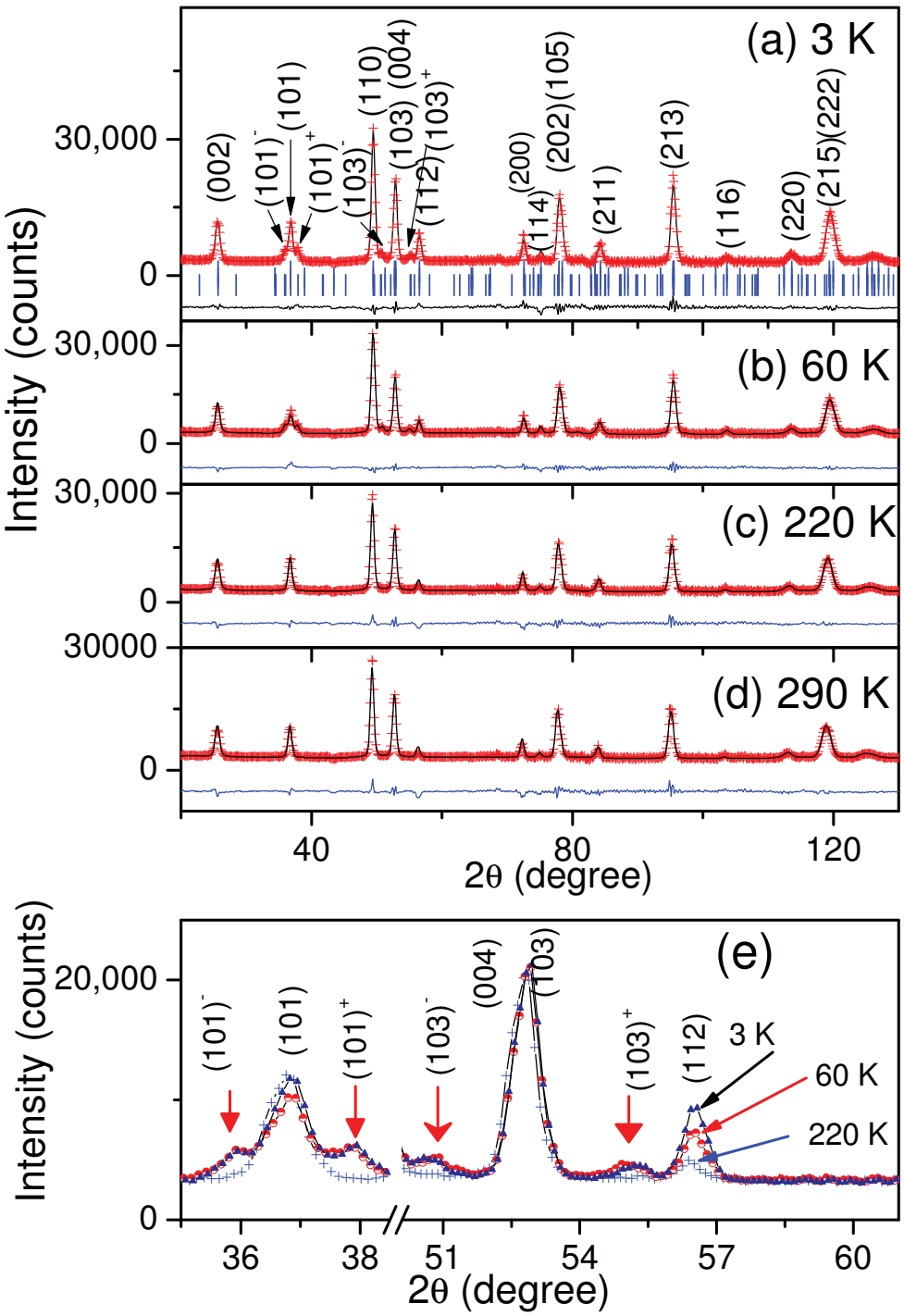
(a) 3 K
(b) 60 K
(c) 220 K
(d) 290 K
(e)
Intensity (counts)
2θ (degree)
(002)
(101)⁻
(101)
(101)⁺
(103)⁻
(110)
(103)
(004)
(112)
(103)⁺
(200)
(114)
(202)(105)
(211)
(213)
(116)
(220)
(215)(222)
3 K
60 K
220 K

Fig. 12

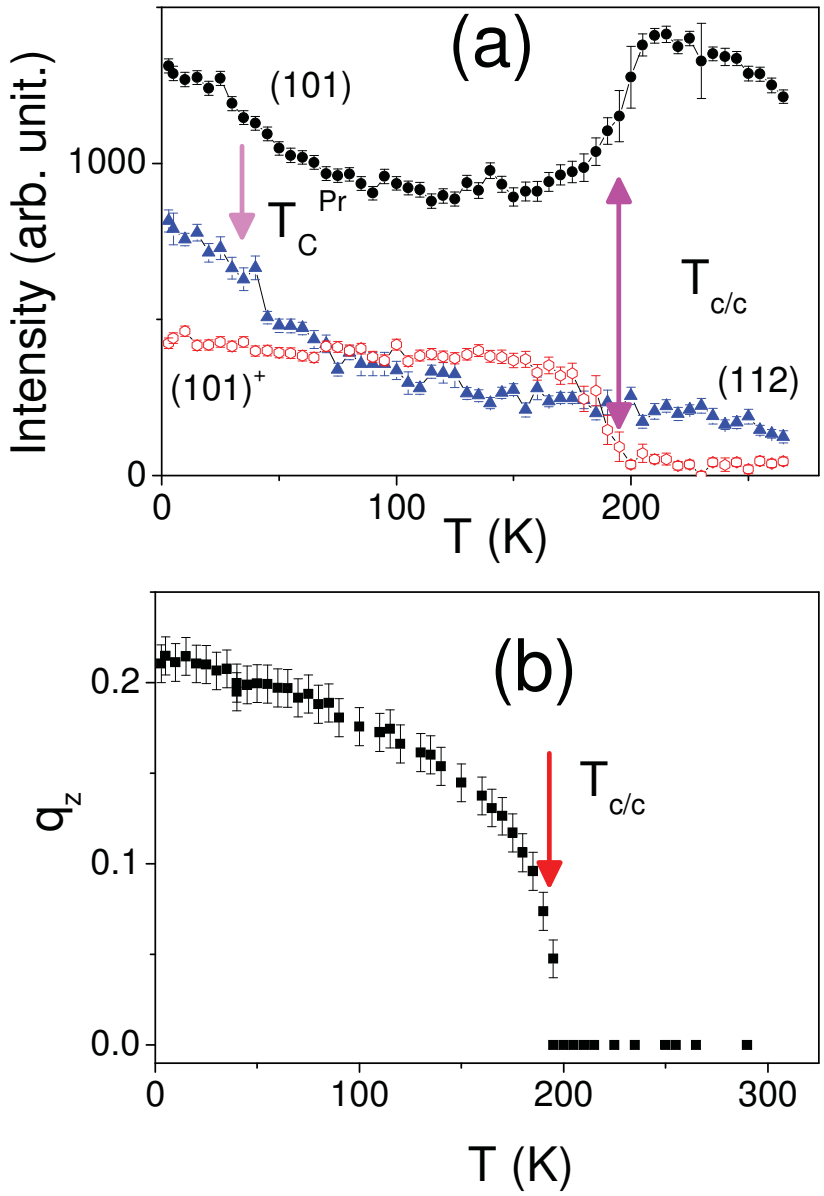
(a)
(101)
Intensity (arb. unit.)
1000
0
T_C^{Pr}
$T_{c/c}$
$(101)^+$
(112)
0
100
200
T (K)
(b)
$T_{c/c}$
q_z
0.2
0.1
0.0
0
100
200
300
T (K)

Fig. 13

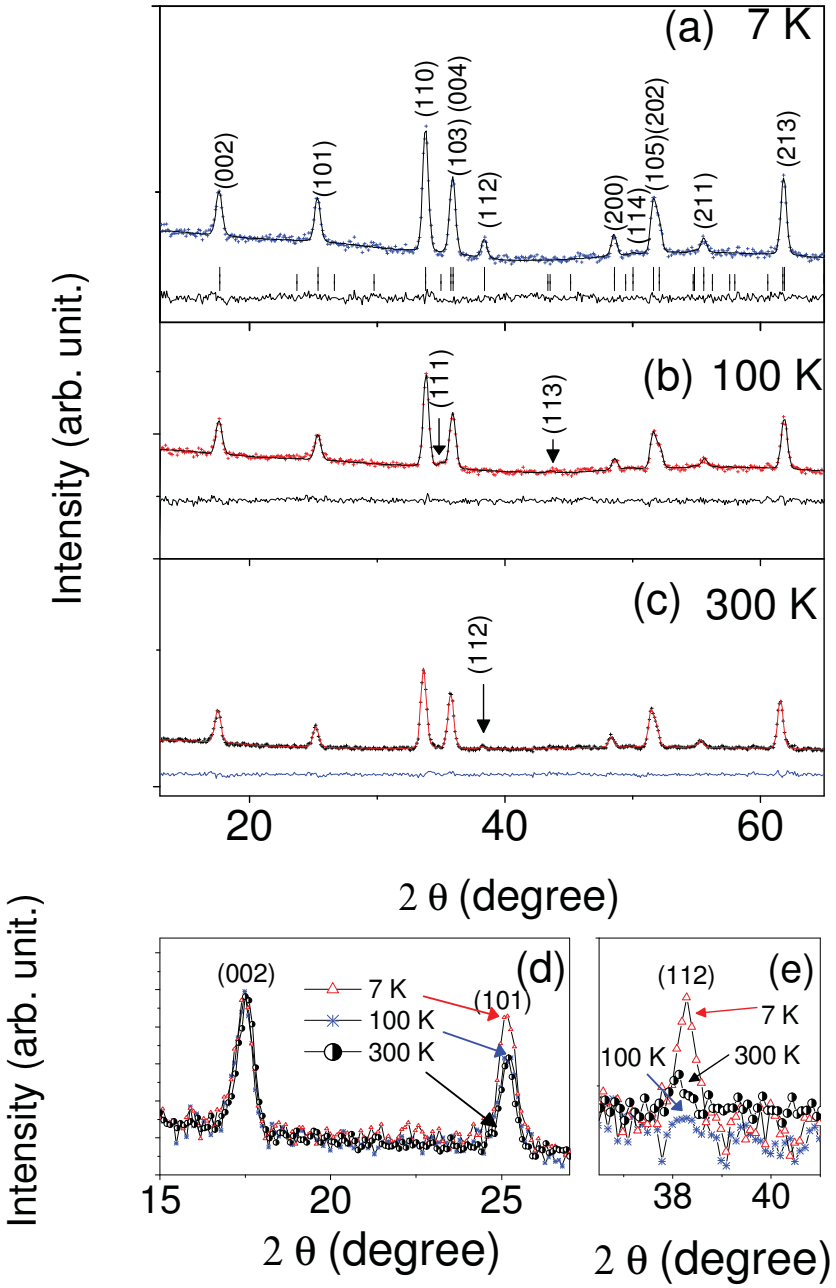
(a) 7 K
(002)
(101)
(110)
(103) (004)
(112)
(200)
(114)
(105)(202)
(211)
(213)
(b) 100 K
(111)
(113)
(c) 300 K
(112)
Intensity (arb. unit.)
20
40
60
2 θ (degree)
(d)
(002)
7 K
100 K
300 K
(101)
15
20
25
2 θ (degree)
(e)
(112)
7 K
100 K
300 K
38
40
2 θ (degree)
Intensity (arb. unit.)

Fig. 14